Appendix:

My Project Details

Project 1: Heavy-Load Robotic Arm for Nursing (2018.6-Now)

I. BRIEF INTRODUCTION

This project is my master project, which belongs to the national key research and development plans. The heavy-load robotic arm is used to carry patients between the wheelchair and the hospital bed. ***The prototype of the manipulator*** is shown in Fig. 1.

My main work is the following three aspects:

1. Structure and Hardware System Design;
2. Tactile Robotic Skin and Safety Control Strategy Design;
3. Proposing two novel torque estimation methods.

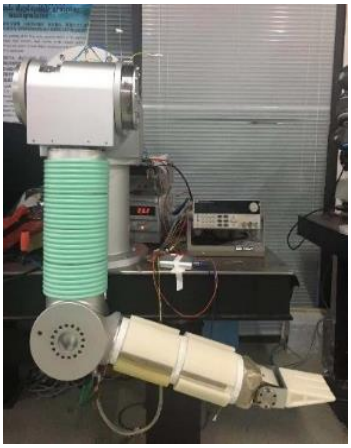

Fig. 1. Prototype of the manipulator arm.

II. MY MAIN WORK

PART-I. Structure and Hardware System Design

Firstly, ***I designed the joint placements*** according to the movement requirement of nursing tasks, as shown in Fig. 2 (a).

I build a dynamic simulation model based on Adams to obtain the maximum load torque of each joint, as shown in Fig.2 (b).

Then I designed the structure of six joints according to the load requirement ***and manufactured the prototype***, as shown in Fig. 2 (c) – Fig. 2 (h).

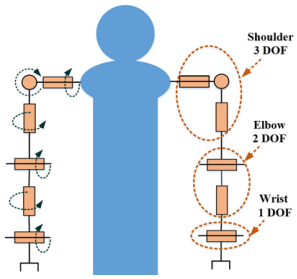

(a) Diagram of robotic arm's joints placements.

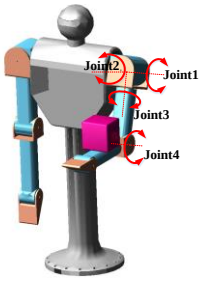

(b) Dynamic simulation model in Adams.

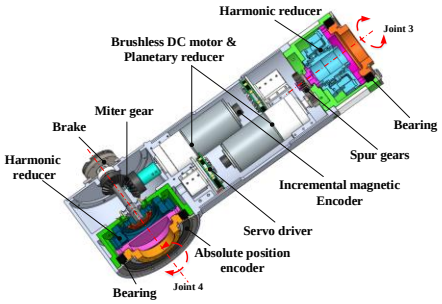

(c) The cross section of the joint 3 and the joint 4

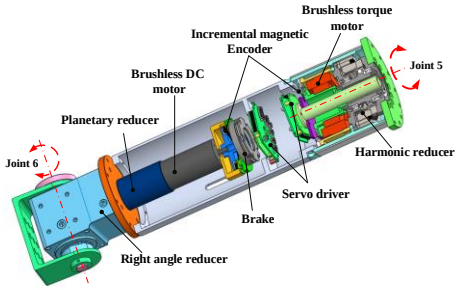

(d) The cross section of the joint 5 and the joint 6

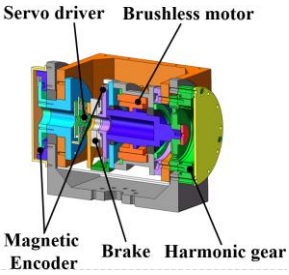

(e) The cross section of the joint 2 (Similar to joint 1)

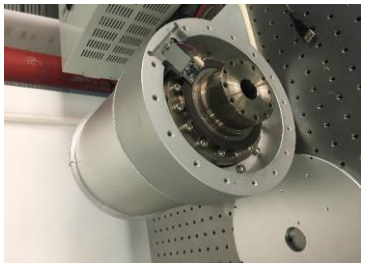

(f) The prototype of the joint 1

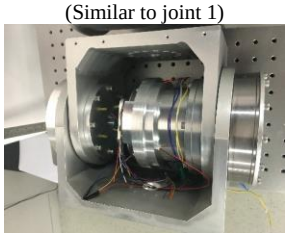

(g) The prototype of the joint 2

(h) The prototype of the joint 3 and the joint 4

Fig. 2. Structural design and prototype manufacturing.

The prototype of the manipulator has the following ***innovations:***

- All joints ***are equipped with high-bearing-capacity harmonic reducer*** to ensure the arm ***can bear load of 50kg.***
- All joints ***are designed to be hollow*** to ensure that the wires can be completely wrapped inside the arm.
- All joints ***are equipped with double high-precision magnetic grating encoders*** (motor side, output side) to ensure high-precision position control.

PART-II. Tactile Robotic Skin and Safety Control Strategy Design

Research Reason: researching the tactile robotic skin is ***to detect the pressure distribution*** on the surface of the manipulator arm, and then ***the results can be applied to safety control strategy***.

Step1: tactile robotic skin design

Firstly, I designed the membrane-structured matrix of piezoresistive flexible film sensors based on the pressure sensitivity of nano-sensitive materials.

To reduce the number of long wires, ***I designed one current signal acquisition board*** for every two pieces of tactile skin which can collect current signals of 64×2 units at the same time, as shown in Fig. 3 (a).

To protect the resistive pressure elements from damage, ***I embed them in pieces of 7mm thick honeycomb skin substrates*** which are processed using photosensitive resin Nitrile Butadiene Rubber (Fig. 3 (b)).

Then I modified the stiffness of the honeycomb substrate by adjusting the thickness and size of the hexagonal cell to obtain ***better performance of shock attenuation.***

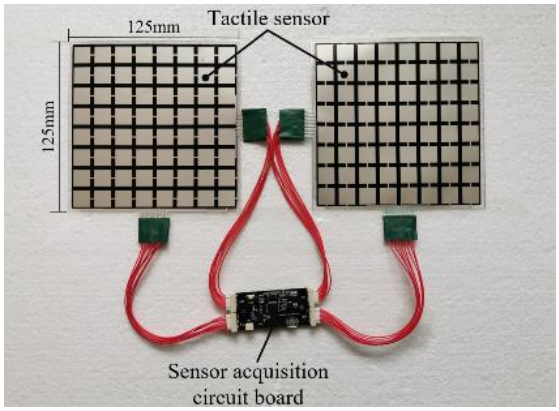

(a) The tactile robotic skin.

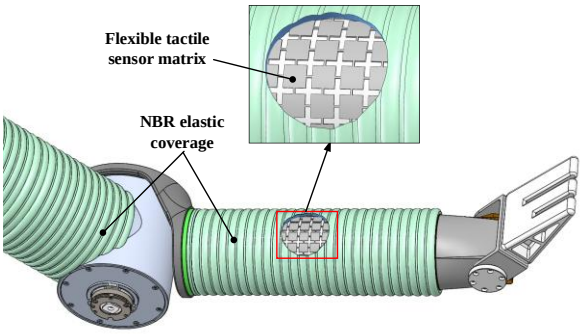

(b) The 7mm thick honeycomb skin substrates.

Fig. 3. The tactile robotic skin and the honeycomb skin substrates.

Step2: performance test

I designed an experiment to calibrate the non-linear relationship between resistance of the pressure sensor unit and pressure**,** as shown in Fig. 4.

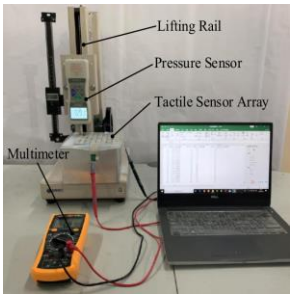

(a) Calibration platform.

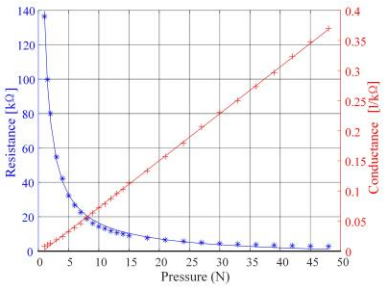

(b) Calibration result.

Fig. 4. Sensor calibration process.

Finally, I tested the performance of the proposed tactile skin by connecting two pieces of the robotic skin on the same plane and placing a weight of 10 kg on them.

The Fig. 5 (b) shows ***the pressure distribution measured by each sensing unit*** and the highest prism represents the calculated center of the load.

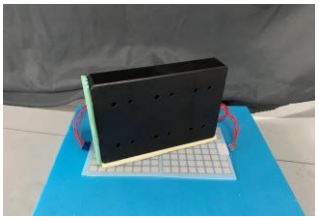

(a) The test platform.

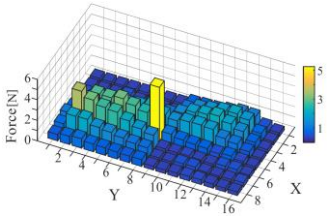

(b) The pressure measurement results.

Fig. 5. Tactile robotic skin performance test.

Step3: hardware system design

I designed hardware system of the whole arm based on CAN-OPEN communication protocol, as shown in Fig. 6.

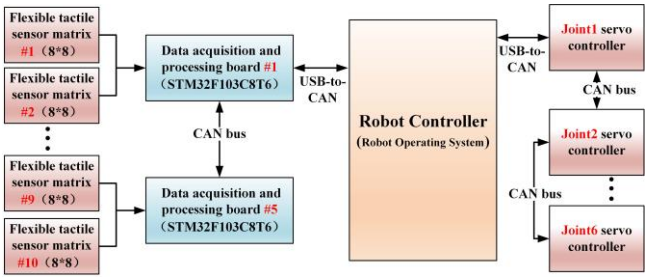

Fig. 6. The hardware system of the manipulator arm.

Step4: safety control strategy

I chose three most dangerous situations for the robotic arm to perform nursing tasks, as shown in Fig. 7.

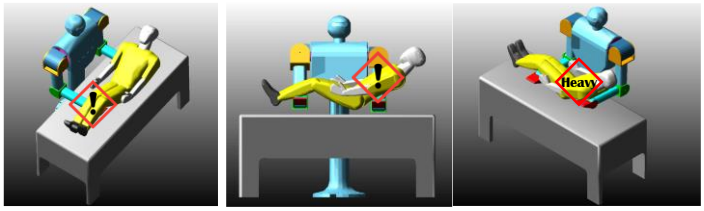

(a) Too far ahead of the arm situation

(b) Too biased towards one side situation

(c) Weight exceeds the payload situation

Fig. 7. Dangerous situations while lifting and transferring patients.

Then I proposed a safety control strategy which can imitate the human mind and make motion decisions, as shown in Fig. 8.

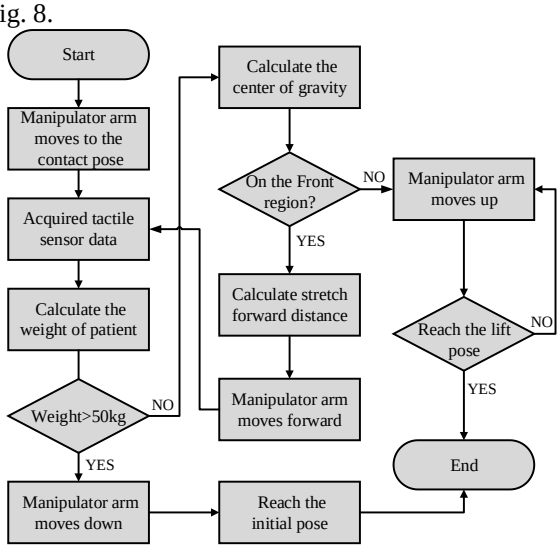

Fig. 8. The flow chart of the safety control method.

Finally, I verified the proposed safety control strategy by pressing the different areas of the manipulator to simulate patient's contact with it, as shown in Fig. 9 – Fig. 11.

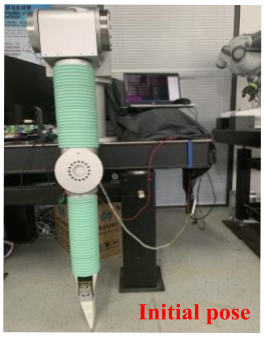

(a) Initial pose

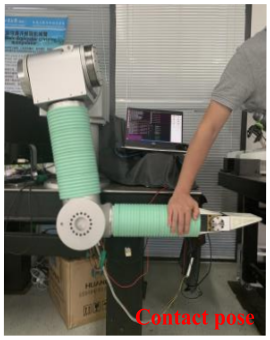

（b）Pressing the front region

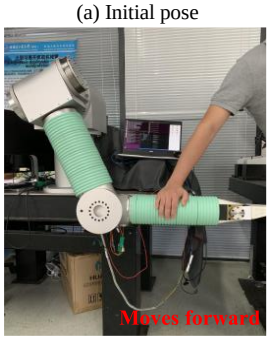

(c) Pressing the center region

(d) Lifting action

Fig. 9. The experimental process of safety control

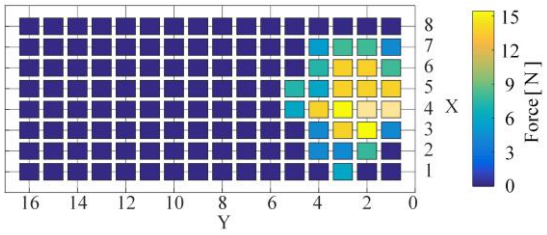

(a) The pressure distribution when pressing the front region

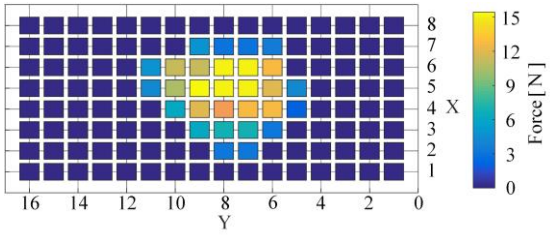

(b) The pressure distribution when pressing the center region.

Fig. 10. The pressure distribution perceived by the tactile skin.

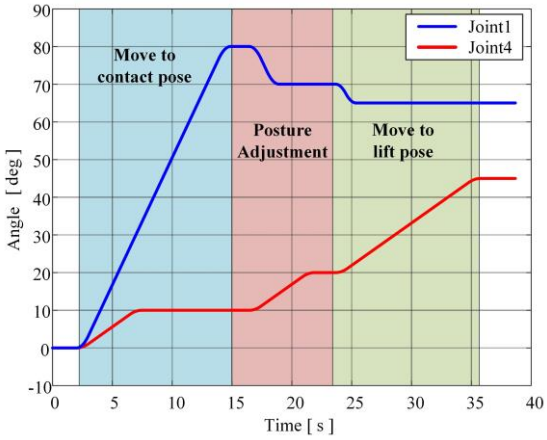

Fig. 11. The angular changes of joint 1 and joint 4

PART-III. Two Novel Torque Estimation Methods

Research Reason: Traditional torque sensors are not suitable for robots in many cases because of the inevitable increase of joint flexibility and joint size. ***I proposed two novel methods*** to estimate torque of robotic joint with harmonic reducer via calibration of its deformation.

(1) Method based on improved deformation modeling

Step1: deformation modeling

Firstly, I experimentally measured the relationship between the total deformation of harmonic reducer and the load.

I found that the relationship has strong nonlinearity and hysteresis (*B* to *B'*), and when the external torque load increases or decreases from different positions (*A*, I_1, I_2, D_1, D_2, *A'*), the curve changes irregularly, as the black solid and dotted lines in Fig. 12.

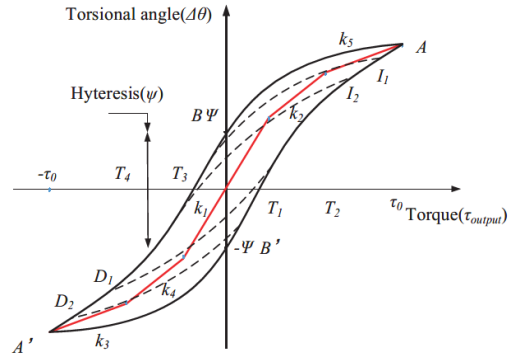

Fig. 12. The relationship between the total torsional angle of harmonic reducer and its output torque.

I divided the harmonic reducer into three deformation units and mark the key deformation position to model the relationship between total deformation and load, as shown in Fig. 13.

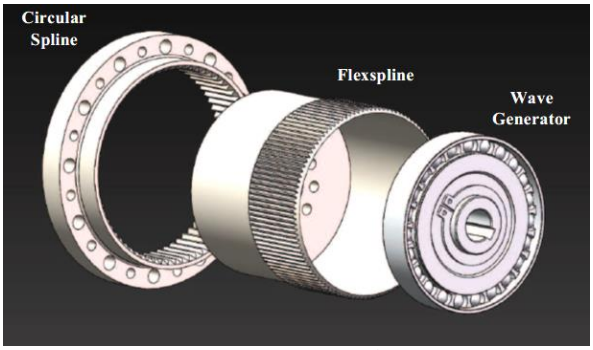

(a) Decomposition structure diagram of harmonic reducer.

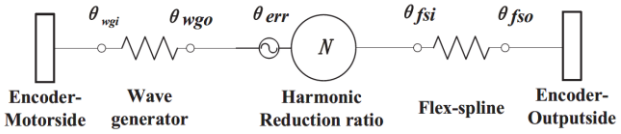

(b) Key angular position in harmonic drive.

Fig. 13. Deformation decomposition and key angular position.

Then I proposed and deduced the total deformation formula of the harmonic reducer, as shown in Fig. 14 (a).

In addition, I designed the fitting formulas for each deformed sub-modules, as shown in Fig. 14 (b) – (c).

$$\theta_{err} = \theta_{fsi} - \frac{\theta_{\omega go}}{N} \tag{2}$$

$$\Delta\theta_f = \theta_{fso} - \theta_{fsi} \tag{3}$$

$$\Delta\theta_\omega = \theta_{\omega go} - \theta_{\omega gi} \tag{4}$$

$$\Delta\theta = \theta_{fso} - \frac{\theta_{\omega gi}}{N} \tag{5}$$

$$\Delta\theta = \Delta\theta_f + \frac{\Delta\theta_\omega}{N} + \theta_{err} \tag{6}$$

(a) Derivation of total deformation formula.

$$\Delta\theta_f = \begin{cases} -k_1\frac{\tau_0}{3} - k_2\frac{\tau_0}{3} + k_3(T_f + \frac{2\tau_0}{3}) & T_f \in [-a \ -b) \\ -k_1\frac{\tau_0}{3} + k_2(T_f + \frac{\tau_0}{3}) & T_f \in [-b \ -c) \\ k_1 T_f & T_f \in [-c \ \ c) \\ k_1\frac{\tau_0}{3} + k_4(T_f - \frac{\tau_0}{3}) & T_f \in [c \ b) \\ k_1\frac{\tau_0}{3} + k_4\frac{\tau_0}{3} + k_5(T_f - \frac{2}{3}\tau_0) & T_f \in [b \ a] \end{cases} \tag{7}$$

$$\Delta\theta_{\omega g} = \omega_0 + \omega_1 I + \omega_2 I^2 + \omega_3 I^3 + \omega_4 I^4 + \omega_5 I^5 + \omega_6 I^6 \tag{8}$$

$$\theta_{err} = a_0 + \sum_{n=1}^{3} [a_n \cos(n\theta_{fso}\omega_{fso}) + b_n \sin(n\theta_{fso}\omega_{fso}) + c_n \cos(n\theta_{wgi}\omega_{wgi}) + d_n \sin(n\theta_{wgi}\omega_{wgi})] \tag{9}$$

(b) Fitting formulas for each deformed sub-modules.

$$\Delta\theta = \begin{cases} h - \frac{\tau_0}{3}k_1 - \frac{\tau_0}{3}k_2 + (T_f + \frac{2\tau_0}{3})k_3 & T_f \in [-a \ -b) \\ h - \frac{\tau_0}{3}k_1 + (T_f + \frac{\tau_0}{3})k_2 & T_f \in [-b \ -c) \\ h + T_f k_1 & T_f \in [-c \ c) \\ h + \frac{\tau_0}{3}k_1 + (T_f - \frac{\tau_0}{3})k_4 & T_f \in [c \ b) \\ h + \frac{\tau_0}{3}k_1 + \frac{\tau_0}{3}k_4 + (T_f - \frac{2}{3}\tau_0)k_5 & T_f \in [b \ a] \end{cases} \tag{10}$$

where a, b, and c are equal to τ_0, $\frac{2\tau_0}{3}$, $\frac{\tau_0}{3}$, respectively, and

$$h = \sum_{n=1}^{3} [a_n \cos(n\theta_{fso}\omega_{fso}) + b_n \sin(n\theta_{fso}\omega_{fso}) + c_n \cos(n\theta_{wgi}\omega_{wgi}) + d_n \sin(n\theta_{wgi}\omega_{wgi})] + k_0 + \frac{1}{N}\sum_{i=1}^{6} I^i\omega_i$$

$$k_0 = \frac{\omega_0}{N} + a_0$$

(c) Total deformation formula of harmonic reducer.

Fig. 14. Formulas in the process of deformation modeling.

Step2: coefficients calibration

I got 18,000 sets of raw data through deformation experiments. The information came from the double encoders installed at the motor-side and the output-side of the joint, and the current was read by the motor driver. ***The variable conversion formulas*** are shown in Fig. 15 (a).

I use the optimal solution as the final calibration result in calibrating the coefficients of the formulas. The SMW method is referred to in the optimization process. ***The main formulas used and deduced*** in the optimization process are shown in Fig. 15 (b).

$$\theta_{wgi} = \frac{\theta_{MEncoder} - \theta_{MEncoderinit}}{R_M} \times 360 \tag{11}$$

$$\theta_{fso} = \frac{\theta_{LEncoder} - \theta_{LEncoderinit}}{R_L} \times 360 \tag{12}$$

$$\omega_{wgi} = \frac{\theta_{wgicurrent} - \theta_{wgilast}}{\Delta t} \tag{13}$$

$$\omega_{fso} = \frac{\theta_{fsocurrent} - \theta_{fsolast}}{\Delta t} \tag{14}$$

(a) Derivation of total deformation formula.

$$\begin{aligned} f(x) &= \|Ax - b\|^2 \\ &= (Ax - b)^T(Ax - b) \\ &= \frac{1}{2}x^T\left(2A^TA\right)x - x^T\left(2A^Tb\right) + b^Tb \end{aligned} \tag{16}$$

$$x^* = \left(A^TA\right)^{-1}A^Tb \tag{18}$$

(b) Objective function of global error and the optimum solution.

$$G_{k+1} = G_k + A_{k+1}^T A_{k+1} \tag{21}$$

$$x^{k+1} = x^k + G_{k+1}^{-1}A_{k+1}^T\left(b_{k+1} - A_{x+1}x^k\right) \tag{22}$$

$$P_{k+1} = P_k - \frac{P_k\alpha_{k+1}\alpha_{k+1}^T P_k}{1 + \alpha_{k+1}^T P\alpha_{k+1}} \tag{25}$$

$$x^{k+1} = x^k + P_{k+1}\alpha_{k+1}^T\left(b_{k+1} - \alpha_{k+1}x^k\right) \tag{26}$$

(c) The iterative equations used in calibrating program.

Fig. 15. Formulas in the process of calibration.

Finally, I got the model coefficients as shown in Fig. 16.

TABLE I
FITTING MODEL COEFFICIENTS OF WAVE GENERATOR COMPONENT AND KINEMATIC ERROR COMPONENT

T_f range	$[-\tau_0 - \frac{2}{3}\tau_0)$	$[-\frac{2}{3}\tau_0 - \frac{1}{3}\tau_0)$	$[-\frac{1}{3}\tau_0 \frac{1}{3}\tau_0)$	$[\frac{1}{3}\tau_0 \frac{2}{3}\tau_0)$	$[\frac{2}{3}\tau_0 \tau_0]$
w_1	-388.278	-2804.237	-6044.592	-68.281	-5449.492
w_2	-749.239	5204.185	4119.795	463.950	-13993.609
w_3	1016.636	3740.866	5439.054	-3366.580	104057.327
w_4	1982.376	-6419.311	-6014.647	-746.738	-151456.711
w_5	991.0376	-5631.224	-2381.304	5430.041	80741.904
w_6	158.3482	-927.7504	2287.355	-2449.350	-14277.104
a_1	-0.0568	0.0696	2.080	-0.0245	0.1833
a_2	-0.1012	0.5732	-2.586	0.0309	-0.1646
a_3	0.01283	-0.0612	1.7197	0.3531	-0.1588
b_1	0.14811	-0.0970	-0.220	-0.1507	0.0463
b_2	0.07148	-0.1757	-0.0064	0.2039	-0.0741
b_3	0.02537	-0.0106	0.2450	-0.0027	0.1218
c_1	0.0515	-0.1775	1.996	0.0113	-0.0501
c_2	-0.0480	0.0608	0.196	0.1082	-0.0618
c_3	-0.0282	-0.1716	1.818	-0.2669	0.00287
d_1	0.0961	-0.1285	0.166	0.0795	-0.0871
d_2	-0.0480	0.0608	0.196	0.1082	-0.0618
d_3	0.0818	-0.0286	0.132	0.0507	-0.0401
k_0^T	38.2570	15.3286	4.7329	5.2152	-8.7800

Fig. 16. Coefficients of each fitting formulas.

Step3: torque estimation

The process of ***using the proposed method to estimate the output torque*** can be divided into two steps, as shown in Fig. 17.

$$\Delta\theta_f = -\sum_{n=1}^{3}[a_n\cos(n\theta_{fso}\omega_{fso}) + b_n\sin(n\theta_{fso}\omega_{fso}) + c_n\cos(n\theta_{wgi}\omega_{wgi}) + d_n\sin(n\theta_{wgi}\omega_{wgi})] + \Delta\theta - k_0 - \frac{1}{N}\sum_{i=1}^{6} I^i\omega_i \quad (27)$$

(a) 1st step: determining the torsional angle of flex-spline.

$$T_f = \begin{cases} (\Delta\theta_f + k_1\frac{\tau_0}{3} + k_2\frac{\tau_0}{3})/k_3 - \frac{2\tau_0}{3} & \Delta\theta_f \in [a\ \ b) \\ (\Delta\theta_f + k_1\frac{\tau_0}{3})/k_2 - \frac{\tau_0}{3} & \Delta\theta_f \in [b\ \ c) \\ \Delta\theta_f/k_1 & \Delta\theta_f \in [c\ \ d) \\ (\Delta\theta_f - k_1\frac{\tau_0}{3})/k_4 + \frac{\tau_0}{3} & \Delta\theta_f \in [d\ \ e) \\ (\Delta\theta_f - k_1\frac{\tau_0}{3} - k_4\frac{\tau_0}{3})/k_5 + \frac{2}{3}\tau_0 & \Delta\theta_f \in [e\ \ f] \end{cases} \quad (28)$$

where a, b, c, d, e and f equal to $-\tau_0, -\frac{1}{3}\tau_0(k_1+k_2), -\frac{1}{3}\tau_0 k_1, \frac{1}{3}\tau_0 k_1, \frac{1}{3}\tau_0(k_1+k_4)$, respectively.

(b) 2nd step: calculating the output torque.

Fig. 17. Using the proposed method to estimate the output torque.

(2) Method based on BP neural network

Step1: selection of input vector elements

I extracted the following variables from the proposed deformation model of the harmonic reducer as the input vector of the BP neural network.

$$Input = [I, \theta_{wgi}, \theta_{fso}, \omega_{wgi}, \omega_{fso}, \Delta\theta]$$

The original current signal is unstable with a large fluctuation amplitude and stochastic noise, so ***I designed a Kalman filter program*** to adjust and correct the current signal, as shown in Fig. 18.

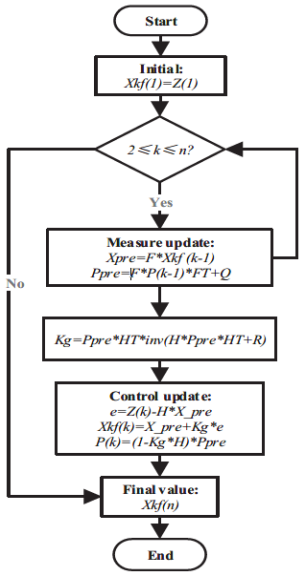

(a) Flow chart of motor current filtering algorithm.

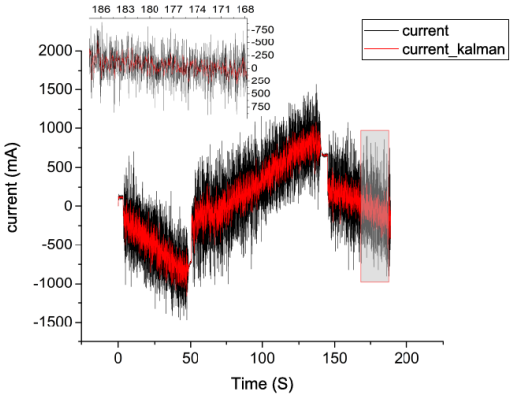

(b) Comparison of current data before and after filtering.

Fig. 18. Adjusting the current signal using the Kalman filter.

Step2: fitting system based on the BP neural network

I built a fitting system based on the BPNN, to approximate the non-linear relationship among the output torque of the harmonic reducer and the measurable input variables.

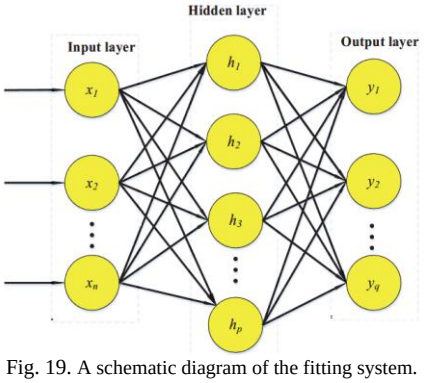

Fig. 19. A schematic diagram of the fitting system.

Then I trained it using sample data obtained from experiments under various conditions, as shown in Fig. 20.

$$x(k) = (x_1(k), x_2(k), \cdots, x_n(k)) \quad (37)$$
$$d(k) = (d_1(k), d_2(k), \cdots, d_q(k)) \quad (38)$$

(a) 1st step: initializing weights and select the input sample.

$$hi_i(k) = \sum_{i-1}^{n} w_{ih} x_i(k) - b_h, h = 1, 2, \cdots, p \quad (39)$$

$$ho_h(k) = f(hi_i(k)), h = 1, 2, \cdots, p \quad (40)$$

$$yi_o(k) = \sum_{h=1}^{p} w_{ho} ho_h(k) - b_o, o = 1, 2, \cdots, q \quad (41)$$

$$yo_o(k) = f(yi_o(k)), o = 1, 2, \cdots, q \quad (42)$$

(b) 2nd step: calculating the input and output of each neuron.

$$E = \frac{1}{2m} \sum_{k=1}^{m} \sum_{o=1}^{q} [d_o(k) - yo_o(k)]^2 \quad (43)$$

(c) 3th step: obtaining global error function.

$$\Delta w_{ho}(k) = -\mu \frac{\partial e}{\partial w_{he}} = \mu \delta_h(k) ho_h(k) \quad (44)$$

$$\Delta w_{ih}(k) = -\mu \frac{\partial e}{\partial w_{ih}} = -\mu \frac{\partial e}{\partial hi_h(k)} \frac{\partial hi_h(k)}{\partial w_{ih}} = \delta_h(k) x_i(k) \quad (45)$$

where

$$\delta_h(k) = \left(\sum_{h=1}^{p} \delta_o(k) w_{ho} \right) f'(hi_h(k))$$

$$\delta_o(k) = (d_o(k) - yo_o(k)) f'(yi_o(k))$$

$$w_{ho}^{N+1} = w_{ho}^{N} + \mu \Delta w_{ho}(k) \quad (46)$$

$$w_{ih}^{N+1} = w_{ih}^{N} + \eta \Delta w_{ih}(k) \quad (47)$$

(d) 4th step: iterating weights

Fig. 20. Training process of the fitting system based on BPNN.

Finally, I estimated the joint output torque by inputting these measurable information, including the motor current, the absolute angular position and angular velocity into ***the well-trained neural network system.***

(3) Experimental test of the proposed two methods

Firstly, I designed the experimental platform.

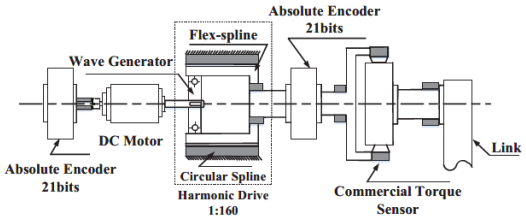

(a) Schematic diagram of experimental platform.

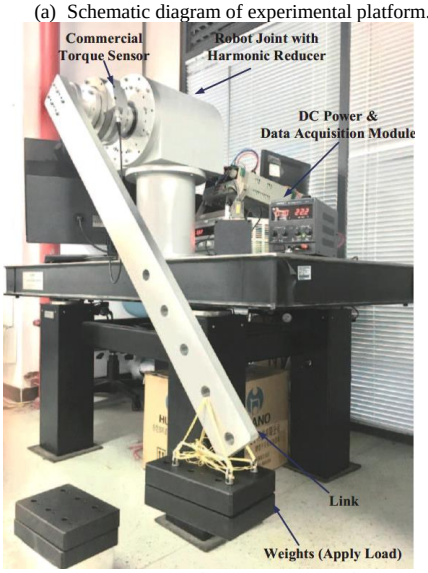

(b) Prototype of experimental platform.

Fig. 21. Experimental setup.

Then I designed four groups of experiments including slow, fast, sudden, and the step-by-step loading processes.

Finally, I got the comparisons of the torque estimation results using the two proposed methods and using the commercial torque sensor, as shown in Fig. 22.

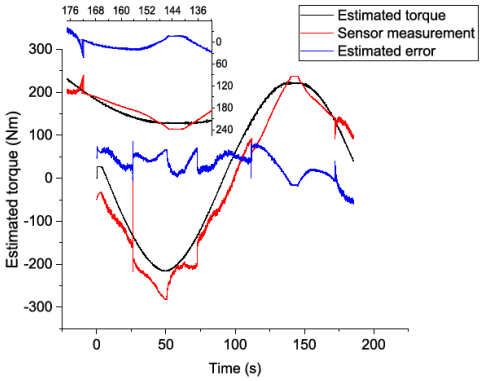

(a) Estimation method based on modeling (slow load change).

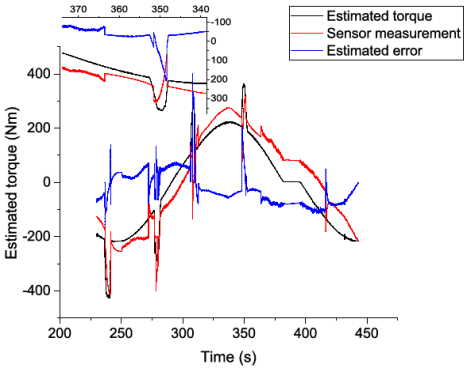

(b) Estimation method based on modeling (fast load change).

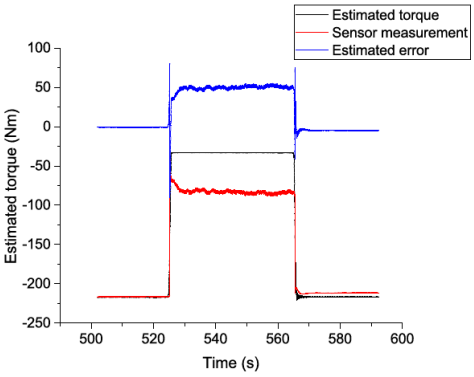

(c) Estimation method based on modeling (sudden load change).

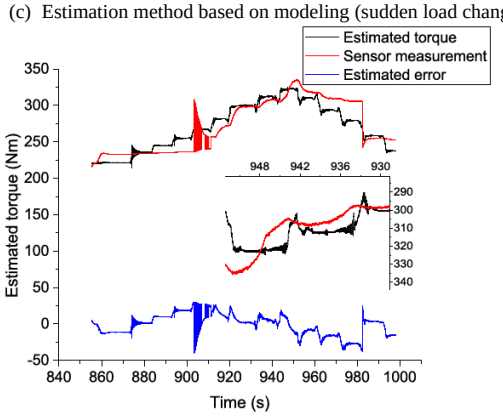

(d) Estimation method based on modeling (static load change)

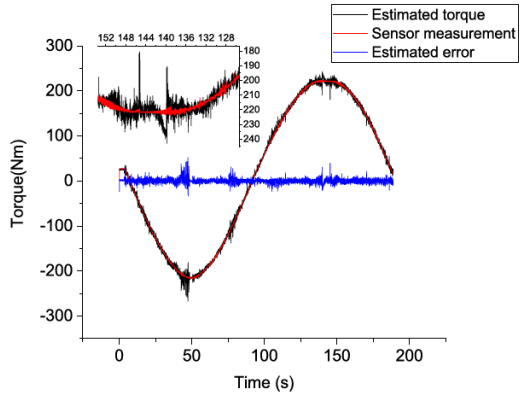

(e) Estimation method based on BPNN (slow load change).

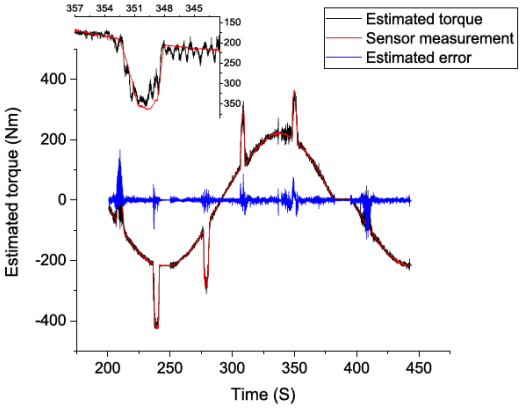

(f) Estimation method based on BPNN (fast load change).

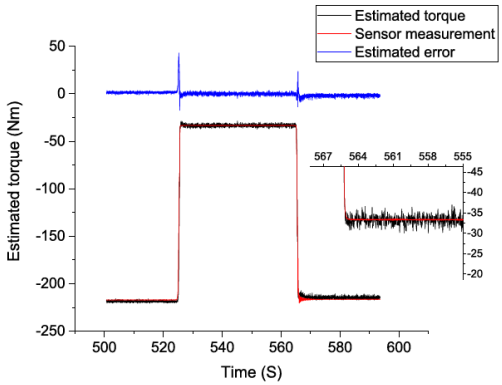

(g) Estimation method based on BPNN (sudden load change).

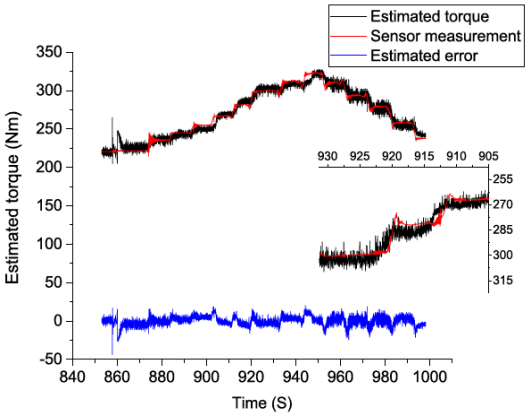

(h) Estimation method based on BPNN (static load change)

Fig. 22. Comparisons of the torque estimation results using the two proposed methods and using commercial torque sensor.

Finally, I compared the performance differences between the two proposed torque estimation methods and ***presented their different suitable application scenarios***, as shown in Fig. 23.

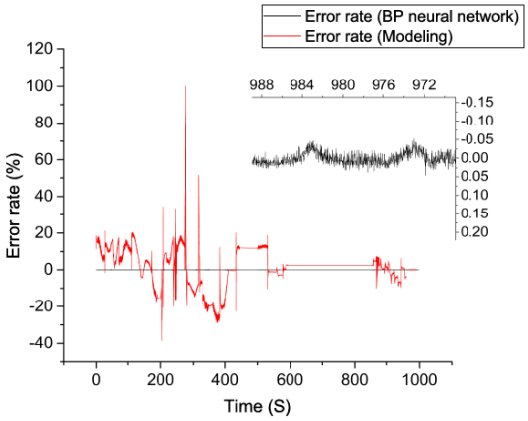

Fig. 23. Error rate comparison of the two proposed methods.

.

II. PAPER PUBLICATION OF THIS PROJECT

[1] **Song, Y. S.**, Huang, H. L., Liu, F., Xi, F. F.*, and Li, B.*, 2019. "Torque Estimation for Robotic Joint With Harmonic Reducer Based on Deformation Calibration". ***IEEE Sensors Journal.*** *(Accept, subject to minor changes)* [PDF]

[2] **Song, Y. S.**, Wu, J. H., and Huang, H. L.*, 2019. "A Novel Heavy-Load Nursing Robotic Arm - Design and Safety Control Based on Tactile Skin". ***IEEE International Conference on Robotics and Biomimetics.*** *(Under review)* [PDF]

[3] Li, B., Wu, J. H., Huang, H. L., **Song, Y. S.**, Liu, F., Ning, Y. H., and Chen, J. A., 2018. "A Novel Kind of 6-DOF Bionic Manipulator Arm". ***C.N. Patent No. 201811515893.8.*** [PDF]

[4] Li, B., Wu, J. H., Liu, F., Xu, W. F., Huang, H. L., **Song, Y. S.**, and Liang, J. L., 2018. "A Novel Kind of Double-arm Robot for Nursing Tasks". ***C.N. Patent No. 201811515894.2.*** [PDF]

Project 2: Cooperative Robots for AI Challenge (2017.9-18.5)

I. BRIEF INTRODUCTION

This project is for ***ICRA 2018 DJI RoboMaster AI Challenge***, which was held by SZ DJI Technology and ICRA 2018 in Brisbane, Australia.

Our team won the runner-up in 48 teams from all over the world.

The basic rules are as follows:

(1) Each team needs to build two robots that can use bullets to battle with other robots, and the projectile hits will be converted into Health Point deduction.
(2) The robots ***must achieve full autonomy*** in obstacle avoidance, target recognition and decision-making.
(3) The winner of the AI Challenge is the team who defeats official robots in shortest time and less HP reduction.

I was leader of navigation group and decision-making group, and ***participated in some work of identification group*** (completed one of our object recognition methods).

My main work is the following 4 aspects:

(1) Improvement of the robotic chassis & Selection of hardware equipment;
(2) Design of an autonomous localization and navigation system based on 2D lidar;
(3) Realization of a real-time detection and tracking system of enemy robots' armor decks based on YOLOv2;
(4) Design of an autonomous decision-making system for the two cooperative robots.

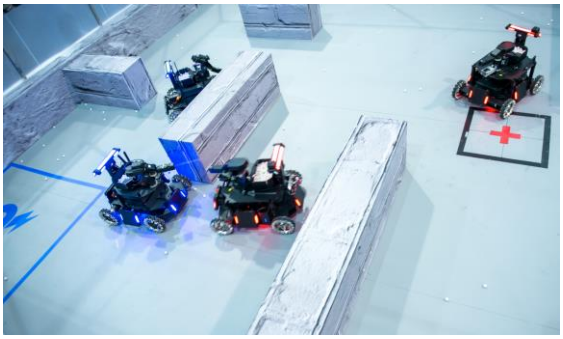

Fig. 1. The live photo of the competition (blue ones belong to our team).

II. MY MAIN WORK

PART-I. Improvement of the robotic chassis & Selection of hardware equipment

I made some appropriate modifications and structural optimization on the basis of the DJI's official robots with my teammates, including:

(1) the design of camera, lidar, mini-computer and other hardware connectors;
(2) the upgrade and reinforcement of chassis structure.

One of the improved robots is shown in Fig. 2.

Fig. 2. One of the improved robots.

On the selection of hardware, I did a lot of research and comparison. Finally, I chose RPLIDAR A2 as the lidar for navigation and mapping, and Nvidia Jetson TX2 as the main processor.

PART-II. Design of an Autonomous Localization and Navigation System

Step1: framework building and programming

Firstly, I built a framework for the navigation system based on ROS, which was composed of Overall node, Global Planner node, Local Planner node, and Localization node.

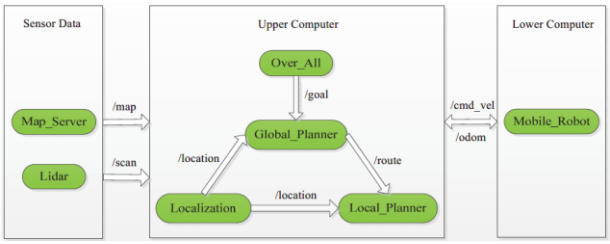

Fig. 3. The framework of the navigation system.

The Overall node is the core node, which receives the goal position from the upper computer and realize the global control of other nodes.

The Global Planner node receives the goal position from Overall node and integrates information from /map and /tf topics to generate global route.

The Local Planner node receives the global route generated by Global Planner node and integrates information from /scan, /odom and /tf topics to calculate control command /cmd-vel.

Similarly, the Localization node subscribes to /map, /tf, and /scan topics and then calculates the location of the robot in real time.

Then I choose the most common sub-algorithms for the Global Planner node, the Local Planner node and the Localization node, which are Dynamic Window Approach algorithm, Timed Elastic Band algorithm and Monte Carlo algorithm, respectively.

Finally, I use C++ to implement the functions of the above ROS nodes. The running processes are shown in Fig. 4.

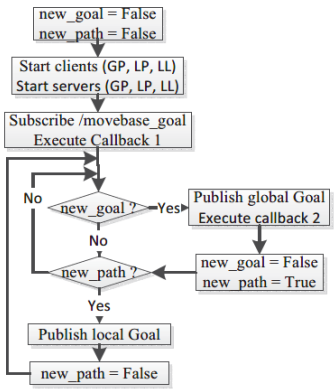

(a) Running process of Overall node.

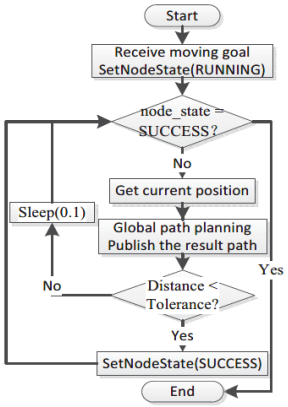

（b）Running process of Global Planner node.

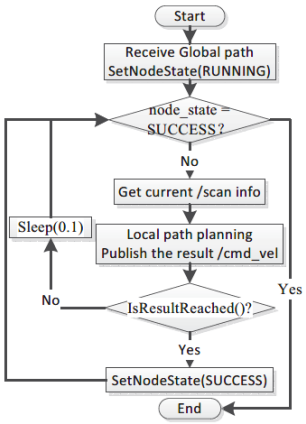

(c) Running process of the Local Planner node.

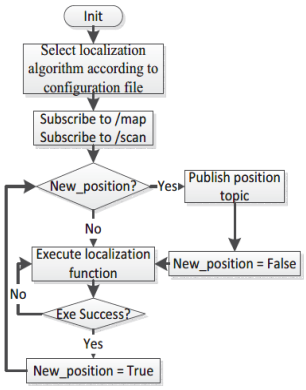

(d) Running process of the Localization node.

Fig. 4. Running processes of these ROS nodes.

In the process of programming, the following two libraries play an important role.

Actionlib of ROS provides a standardized interface for preemptable tasks such as moving the base to a target position, performing a laser scan and returning the resulting point cloud, etc.

Protocol buffers are Google's platform-neutral extensible mechanism for serializing structured data. It automatically generates a series of library functions which greatly facilitate users to read and write custom configuration files.

Step2: Simulation verification

Firstly, I used ROS stage to configure a simulated robot which is equipped with lidar, camera and other sensors, ***and set up the same map environment*** as the competition venue.

It has the ability to publish and subscribe to topics like a real robot, as shown in Fig. 5.

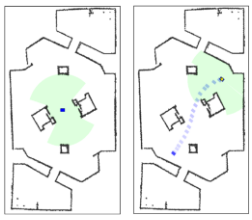

(a) Subscribing to the /cmd_vel topic.

（b）Publishing the /scan topic.

Fig. 5. Functional verification of the simulated robot.

Then I verified the effectiveness of this navigation system by setting a goal position in the upper right corner of the simulation environment. The experimental results of its global path planning, local path planning and real-time localization are shown in Fig. 6.

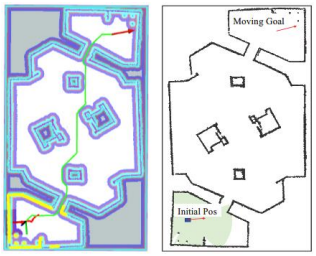

(a) The global planning and local planning results.

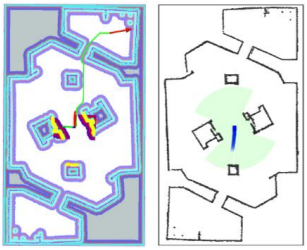

（b）The real-time localization result.

Fig. 6. Simulation results of the navigation algorithm.

Step3: Experimental verification

I built an experimental site with some of my teammates, to verify the effectiveness of our navigation algorithm, as shown in Fig. 7.

Testing videos:

[Navigation displayed in rviz]

[Navigation in real scene]

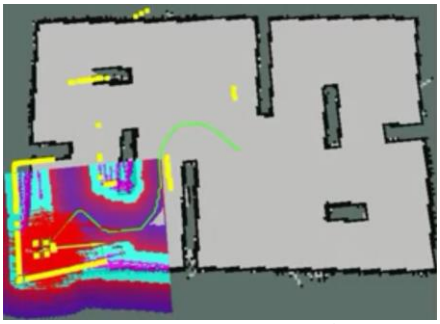

(a) Path planning displayed in rviz of Ubuntu 16.04.

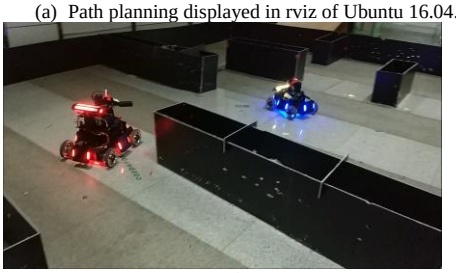

(b) Prototype of experimental site.

Fig. 7. Experimental validation of the navigation algorithm.

PART-III. Design of an autonomous decision-making system for the two cooperative robots

I designed five working modes for the automatic decision-making system of the robots based on these information, as shown in Fig. 8.

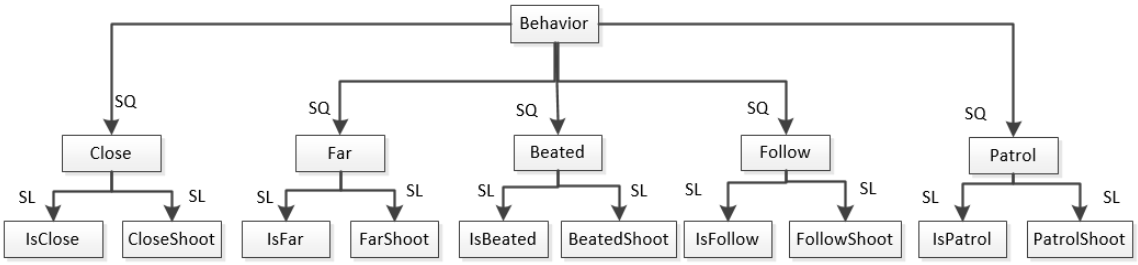

Fig. 8 Basic structure of behavior tree in the decision system.

Closeshoot mode: this mode means that the distance from one of the enemy robots is less than 1.5m. In this case, the robot will rotate to a position 30 degrees from the enemy and keep shooting continuously.

Farshoot mode: this mode means that the distance from one of the enemy robots is more than 1.5m. In this case, the robot will move close to the enemy, and keep single shoot until entering the closeshoot mode.

Patrol mode: this mode means that neither of our robots detect the enemy. In this case, the robot will patrol the 6 pre-set points until one of the enemies is detected. [Video]

Beated mode: this mode means that the robot detects that its armor plate is being beat. In this case, the robot will rotate until the enemy is detected. [Video]

Follow mode: this mode means that one of our robots does not detect any enemy, but the other robot does. In this case, the robot will move to the position sent by the other robot, and patrol until it also detects the enemy. [Video]

I used the decision tree to implement the autonomous decision-making system, and ***the Pitree***, an open source library in Python was used in programming.

Fig. 9. The experimental verification of the beated mode.

PART-IV. Realization of a real-time detection and tracking system based on YOLOv2

We use two methods for target recognition.

- The main camera uses the traditional feature recognition method.
- Aided cameras use YOLOv2-based image segmentation method.

I participated in the latter part and realized the recognition of enemy robots using open source YOLOv2, as shown in Fig. 10.

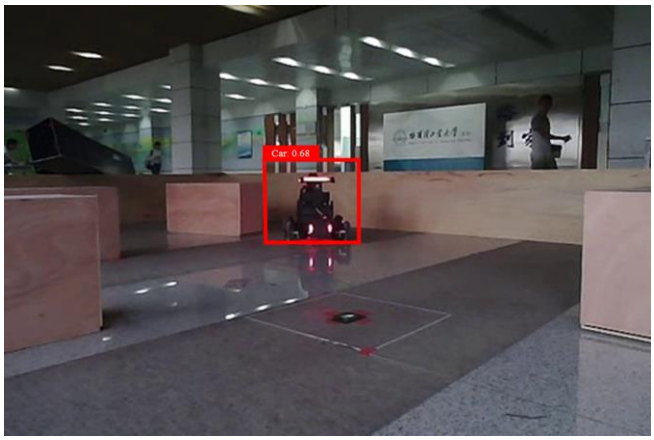

Fig. 10. Recognition of enemy robots using YOLOv2.

III. PAPER PUBLICATION OF THIS PROJECT

[1] **Song, Y. S.**, Zhang, T. S., Li, B.*, 2018. "A Virtual Experiment Platform for 2D Robot Autonomous Navigation Algorithm System". ***IEEE International Conference on Information and Automation.*** pp. 989-994. [PDF]

Project 3: Commercial 3D Printers (2015.9-17.6)

I. BRIEF INTRODUCTION

This project came from a startup I co-founded with my classmates in my junior and senior years.

It focused on the field of 3D printing technology, designing and manufacturing FDM 3D printers, chocolate 3D printers and providing technical support related to 3D printing.

My main work is the following 4 aspects:

(1) Structural design and manufacture of our first generation FDM 3D printer;
(2) Proposed a novel extrusion & heating system specialized for chocolate printing;
(3) Solved the tricky plugging problem by many chocolate melting experiments;
(4) Designed a 3D printing training center for a vocational school.

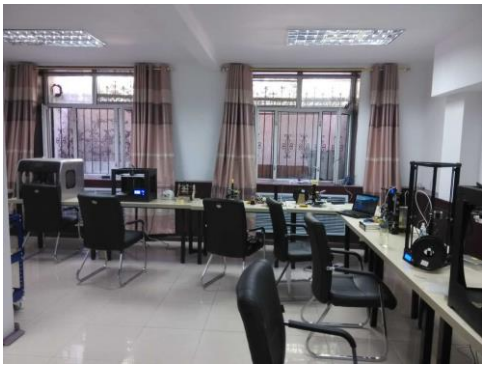

Fig. 1. The environment of our small startup.

II. MY MAIN WORK

PART-I. Structural design and manufacture of our first generation FDM 3D printer

I designed the structure and the appearance of our first FDM 3D printer.

Its motion form is X-Y-Z type, which ***can achieve the same printing accuracy (0.1mm)*** as the commercial printers sold on the market at that time. Its 3D model and prototypes are shown in Fig. 2.

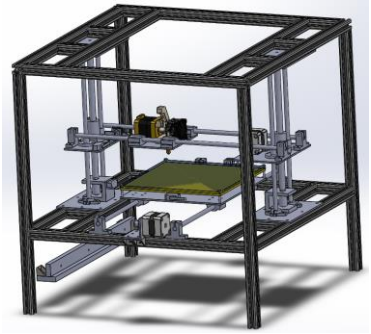

(a) 3D model of our first generation of FDM 3D printer.

(b) Prototype of our first generation of FDM 3D printer.

Fig. 2. Prototype of our FDM 3D printer after packaging.

PART-II. Proposed a novel extrusion & heating system specialized for chocolate printing

I proposed and designed a novel extrusion and heating system specialized for chocolate printing, which utilized a screw to extrude the melt chocolate stored in the syringe. Its 3D models and prototype are shown in Fig. 3.

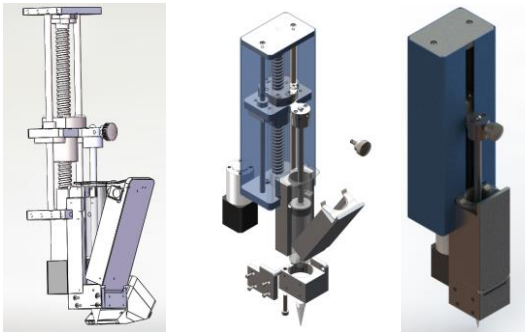

(a) 3D model & Assembly explosion diagram & Rendering diagram.

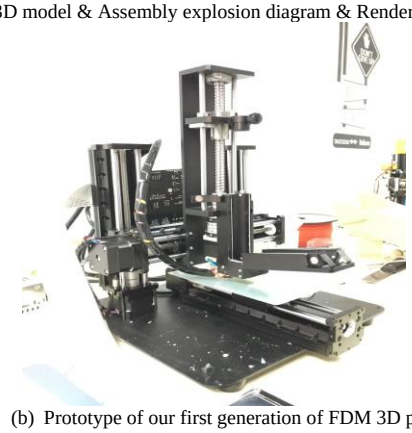

(b) Prototype of our first generation of FDM 3D printer.

Fig. 3. Prototype of our chocolate 3D printer.

PART-III. Solved the tricky plugging problem by many chocolate melting experiments

The chocolate 3D printers ***faced a common problem -- plugging problem***, because of the existence of impurities, extrusion head temperature change and other factors.

I finally solved this tricky problem through many times of melting experiments, including adjusting the composition ratio, melting temperature, extrusion speed and other factors.

Fig. 4. The melting pot used in these experiments.

PART-IV. Designed a 3D printing training center for a vocational school

My team members and I designed a 3D printing training room for a vocational and technical school, and ***produced 10 class-hours teaching materials*** for them, including the design and manufacture of 3D printers, the commercial application of 3D printing, etc.

The rendering diagram of the training room is shown in Fig. 5.

(a) Horizontal Perspective.

(b) Vertical Perspective.

Fig. 5. The rendering diagram of the training room.

III. OTHER RECORDS OF THE STARTUP

Some of our small startup's products, honors, and working environment are shown below.

(a) Honorary Certificates & 3D Printing Products.

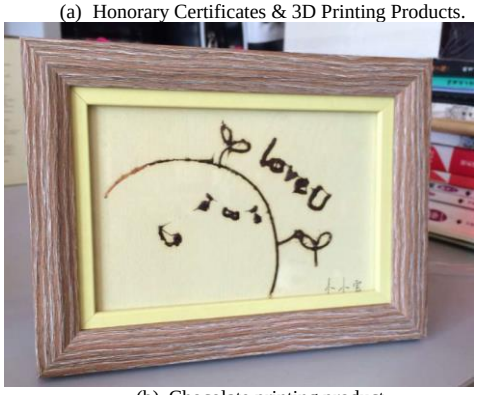

(b) Chocolate printing product.

(c) Our conference room.

Fig. 6. Other records of our small startup.